Comparison of Numerical Simulations and Laboratory Studies of Shock Waves and Cavitation Bubble Growth Produced by Optical Breakdown in Water

E. J. Chapyak and R. P. Godwin

Applied Theoretical and Computational Physics Division
Los Alamos National Laboratory
Los Alamos, New Mexico 87545

Alfred Vogel
Medizinisches Laserzentrum Lübeck GmbH
D-23562 Lübeck, Federal Republic of Germany

ABSTRACT

In numerical calculations of idealized bubble dynamics test problems, Los Alamos computational tools perform well. A realistic equation of state must be used and geometrical features must be carefully modeled to simulate experiments accurately. In this work, we compare numerical simulations taking these features into account with experiments performed at the Medizinisches Laserzentrum Lübeck. We compare the measured and calculated positions of the shock front and of the bubble wall as a function of time in the laser optical breakdown of water produced by 30-ps 1-mJ Nd:YAG laser pulses.

Keywords: bubble dynamics, cavitation, experimental and numerical hydrodynamics, shocks, acoustic radiation, laser medical applications

1. INTRODUCTION

Bubble dynamics and its associated shock and acoustic waves and jetting are important in laser medical applications. The dynamics produces both intended medical effects and undesirable collateral effects. Medical treatments in which bubble dynamics is an issue include mature procedures, such as intraocular laser surgery,[1] and procedures, such as laser thrombolysis,[2] in development. Multidimensional Eulerian compressible hydrodynamics codes capably model shock waves and highly distorted flows. Such codes together with appropriate laser absorption models, material equations of state (EOS), and tissue dynamics and failure models can aid in understanding and optimizing clinical protocols in which bubble dynamics is an important consideration. We have demonstrated the efficacy of the Los Alamos National Laboratory (LANL) code MESA-2D for the purely hydrodynamic issues of bubble dynamics.[3]

Vogel *et al.*[1] used time-resolved photographic methods to investigate shock wave and cavitation bubble expansion after optical breakdown in water with Nd:YAG laser pulses of 30-ps and 6-ns duration and energies typical of medical applications. They measured the position of the shock front and bubble wall position as a function of time with temporal resolution ~1 ns and spatial resolution ~4 μm. These high-resolution measurements provide excellent data for quantitative comparison with numerical simulations.

We simulate the dynamics of 1-mJ 30-ps laser pulses for comparison with the experimental data obtained at the Medizinisches Laserzentrum Lübeck (MLL); 30 ps is sufficiently short that hydrodynamic motion during the laser-energy deposition can be ignored. Significant pressure relaxation will occur over a time $\tau \approx R_o / u_S \approx R_o / 2c_o \approx 70$ ps, where R_0 is the initial plasma radius (~20 μm); u_S is the initial shock velocity and $c_0 = 1.5$ km/s the sound velocity in water; 1 mJ is well above the plasma breakdown threshold allowing us to finesse complexities associated with laser-matter coupling near the threshold.

Vogel *et al.* used the size of the initial laser plasma and of the maximum bubble, which are easily measured quantities, together with approximate theoretical models to analyze their experiments. Their calculations produce useful physical insight into the dynamics. However, as Vogel *et al.* acknowledge, weaknesses of the theoretical model assumptions, the non-spherical geometery of deposition, and the inadequacy of the equations of state used are limitations of their numerical calculations. Similar limitations apply to recent calculations of laser and electrical spark cavitation.[4,5] The cited studies use

approximate equations of state in functional form and approximate theories that derive from the classic work of Kirkwood and Bethe.[6] In contrast, we use tabular EOS information derived from experiment and our MESA-2D Eulerian hydrodynamics code[3] to simulate the MLL experiments. By doing so, we avoid compromising model approximations. Energy is deposited in an initial plasma volume estimated from the MLL observations, and this energy, together with the numerical tools, produces the plasma and subsequent bubble dynamics.

Laser-produced bubble dynamics is an excellent example of a physical phenomenon for which experimental and numerical studies complement one another when appropriately used together. Diagnostic measurements during the initial bubble dynamics (and at subsequent bubble collapses) are difficult. The small size and rapid temporal changes in the region over which a shock occurs make measurements of this important feature of bubble dynamics particularly difficult. On the other hand, in numerical simulations we can use fine spatial and temporal zoning over the limited parameter space where high pressures and shocks are important. The maximum bubble size is easily measured experimentally. However, multidimensional Eulerian computations of the entire bubble history are expensive and time consuming. This is the case since, near its maximum size, the bubble is very large compared to its initial size and is moving slowly, making fine computational resolution costly.

Simulations of the MLL experiments test our hydrodynamics algorithms and the water EOS used with them. The water EOS is particularly critical in determining the pressure driving the dynamics.[7] The bubble pressure $p \sim E_I / V$, where E_I is the internal energy and V the volume. To describe the internal energy in the laser breakdown plasma realistically, the EOS must properly account for the heat of vaporization of water and the high energy cost of ionization. The ratio of water vapor volume to liquid water volume is $\sim 10^3$, except close to the critical point. Thus the instantaneous vaporization of water at 1 bar can easily produce kilobar pressures. The SESAME EOS tables[8,9] we have used include the effects of both phase changes and ionization.

2. INITIAL CONDITIONS FOR THE SIMULATIONS

In modeling the 30-ps laser-breakdown experiments, we assume that there is instantaneous deposition throughout the breakdown volume and that the resulting initial pressure is uniform throughout that volume. Using the 2 ns frame of Fig. 1 (Fig. 3 of Ref. 1), we approximate the deposition region with a cylindrically symmetric volume. The volume consists of two cones with their bases in contact. We place the bases at the location of the maximum radial extent of the initial plasma. We chose this initial plasma geometry for simplicity and because the dynamics is strongly dependent upon the initial volume but not its exact shape. (Our computational tools allow us to model arbitrary shapes and even 3-D figures, but the associated complexity is not warranted for these simulations.) The assumed initial volume

$$V_0 = \frac{\pi}{3} R_0^2 \left(b_{ds} + b_{us} \right),$$

where R_0 is the initial plasma radius and b_{ds} and b_{us} are the "downstream" (that is, away from the laser) and "upstream" cone heights, respectively. The values of the these parameters cannot be obtained directly from Fig. 1, since that photograph was made ~2 ns after the laser deposition and after significant dynamic growth. Nevertheless, the figure, together with the known focal plane and focal cone of the incident laser light, allows us to estimate R_0, b_{ds}, and b_{us}. The spatial and temporal resolutions of the photograph limit the acceptable parameter values. (We have ignored the narrow needle of plasma near and downstream from the focal plane. This needle, which results from the diffraction focal neck and perhaps self-focusing, contains very little volume and energy.) Vogel *et al.* have measured the bubble and shock radius as a function of time at the axial location we have chosen for R_0. These measurements allow us to estimate the value of the initial radius by extrapolating back to the time at which we assume instantaneous deposition of the absorbed laser energy; R_0 is a particularly important initial parameter since the initial volume is proportional to its square and the MLL measurements were made at its axial location. We assume that the maximum radial bubble wall and shock locations are both R_0 at the computational time zero. We have chosen for the initial computational conditions $R_0 = 21$ μm, $b_{ds} = 171$ μm, and $b_{us} = 103$ μm yielding an initial volume $V_0 = 1.265 \times 10^{-7}$ cm^3. Our choices for the computational spatial zoning and temporal steps are generally smaller than the diagnostic resolution of the MLL experiments. At radii less than 100 μm, the computational zones are square with $\Delta r = \Delta z = 1$ μm. At larger radii Δr and Δz are expanded geometrically by a multiplicative factor of 1.1 out to 1264 μm.. The total number of computational cells is 4.5×10^4. A problem takes a few minutes to run on a CRAY T-90.

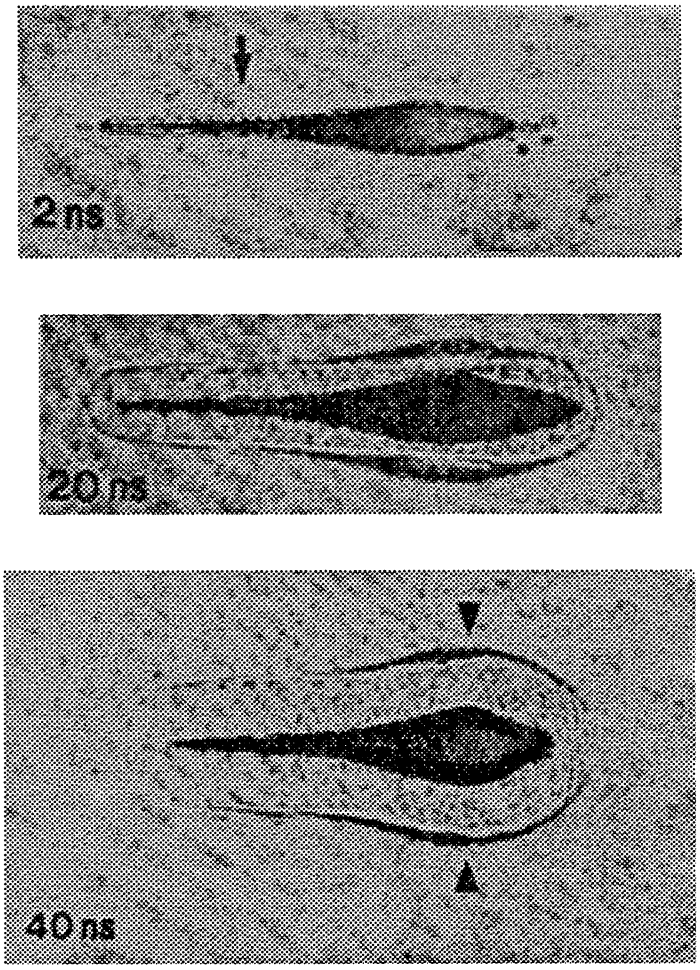

Fig. 1. Photographic records of the shock wave and bubble wall motion after the optical breakdown of water by a 30-ps 1-mJ laser pulse in the MLL experiments. (The photos are not reproduced to exactly the same scale.)

We have used the best tabular water EOS information available to us. For water outside the initial energy deposition region, we used an EOS based upon NIST data[9] (SESAME #7152). That EOS does not extend into the region of thermodynamic coordinates produced within the deposition volume. In that volume, we have used another LANL EOS (SESAME #7150). SESAME 7152 is a non-equilibrium EOS, whereas 7150 is an equilibrium, Maxwell construction, EOS. We chose the initial computational conditions to ensure that, before deposition of the absorbed laser energy, there is no numerical dynamics at a pressure of one atmosphere and a temperature of 30°C. Our simulations do not include the effects of viscosity or surface tension. Estimates indicate that these effects are negligible in the problem posed. In the 30-ps 1-mJ MLL experiments, 0.76 mJ is deposited in the laser-breakdown volume.[10] We have therefore deposited 0.76 mJ in the volume V_0 to initiate the simulation dynamics. This energy, together with the EOS, produces a 42.968 kbar (4296.8 MPa) pressure and 2163°K temperature.

3. COMPUTATIONAL RESULTS AND COMPARISONS TO EXPERIMENT

In Fig. 2, we have plotted the computed and measured maximum radial shock wave and bubble wall location as a function of time. The agreement between experiment and simulation is extremely good, although the simulated shock is slightly outrunning the measured shock. This slight disagreement is not surprising, since the shock wave and bubble wall dynamics are driven rather differently. The initial pressure created by the energy deposition launches the shock wave, while the entire pressure history within the bubble influences the bubble wall motion.

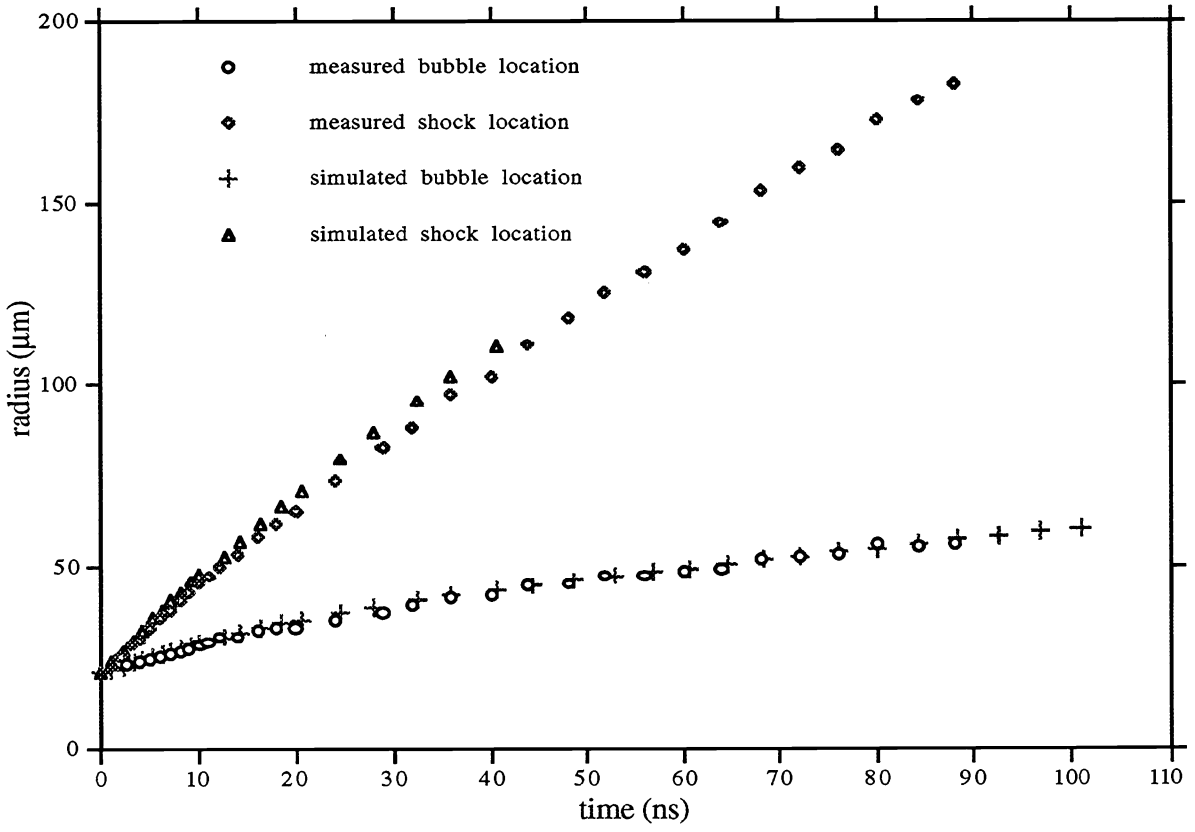

Fig. 2. Measured and computed locations of the shock wave and bubble wall as a function of time after the laser deposition.

Figure 3 displays the calculated radial pressure profile in the plane of the maximum shock wave and bubble radius at 5, 10, 20, 40 and 80 ns. The pressures are typically ~ 10^{-2} Mbar (1000 MPa). For times greater than about 10 ns, the peak pressure is near the advancing shock front. A physical shock is very sharp. The shock front of Fig. 3 is numerically broadened over several computational zones. The computational zone size is 1 μm for radii less than 100 μm (0.01 cm) and increases slowly at larger radii. The numerical broadening is significant for all the profiles of Fig. 3, but is greatest at the radii where we have used the largest computational zones. Comparing Fig. 3 with Figs. 9 and 11 of Ref. 1 shows that, for times greater than approximately 5 ns, our simulations of both the pressure profiles and shock location agree quite well with the model predictions of Vogel *et al.*

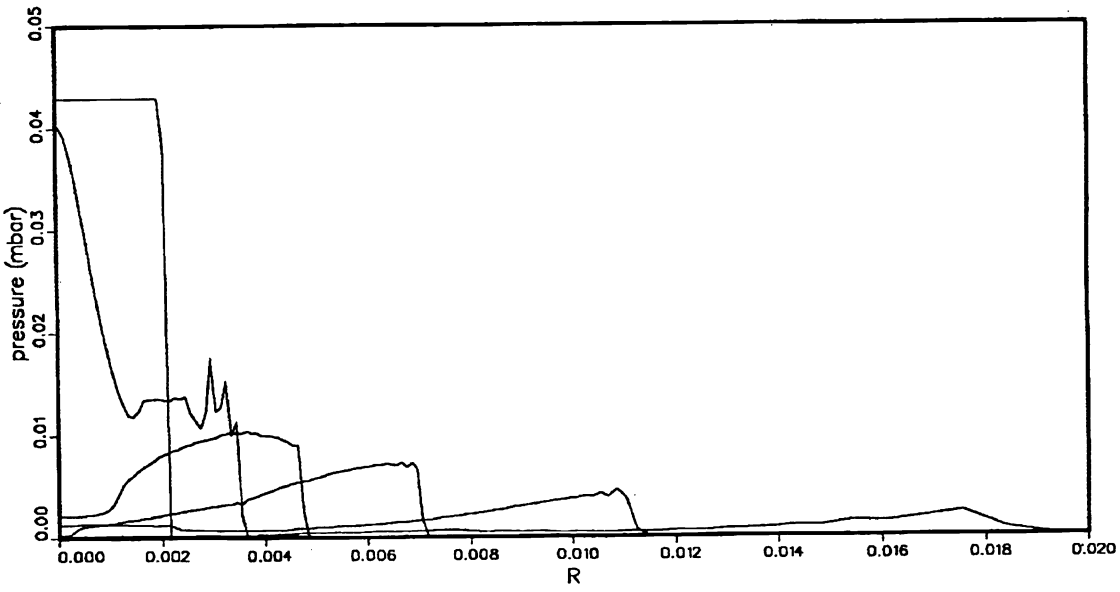

Fig. 3. Computed radial pressure profile in the plane of the maximum shock wave and bubble wall radius at 0, 5, 10, 20, 40 and 80 ns. A physical shock is very sharp. The numerical shock front is broadened over several computational zones. The computational zone size is 1 μm for radii less than 100 μm (0.01 cm) and increases slowly at larger radii.

The principal purpose of our simulations was the quantitative comparison with MLL experimental data presented in Fig. 2. We are also interested in comparing the two-dimensional simulation features with the experiments. In Fig. 4, we display the numerical shock wave location and bubble wall contours at the computational times 2, 20, and 40 ns for comparison with the photographic records of Fig. 1 and Ref. 1. An extremely sharp pressure discontinuity exists at a shock wave front. In simulations, the numerical algorithms smear this discontinuity over a few computational zones. We have chosen to represent the shock front by plotting the 100 bar (10 MPa) isobar. The bubble wall is the interface of the volumes represented by the two water equations of state. With the exception of the axial volume near the focal plane, the two-dimensional experimental and numerical shock wave contours compare favorably. (Small changes in our assumed initial plasma shape could bring the contour plots and photographs into excellent agreement without compromising the quantitative agreement of Fig. 2.)

The distribution of energy provides insight into the relative importance of various physical processes in the dynamics. In Table I, we list the energy in various energy channels at selected simulation times.

Table I. Computational distribution of energy at selected times.

t (ns)	IE_I (mJ)	ΔIE_I (mJ)	IE_O (mJ)	ΔIE_O (mJ)	KE_I (mJ)	KE_O (mJ)
0	0.764128*	0.760	1421.92	0.00	0.0000	0.000
2	0.683595	0.679	1421.95	0.03	0.0219	0.039
20	0.470244	0.466	1422.05	0.13	0.0076	0.149
40	0.432914	0.429	1422.08	0.16	0.0079	0.157
60	0.414173	0.410	1422.09	0.17	0.0074	0.161
100	0.392142	0.388	1422.10	0.18	0.0025	0.173

* After deposition of the 0.76 mJ of absorbed laser energy to initiate dynamics.

The interpretation of Table I. requires explanatory comments. We have carefully chosen the computational conditions so that there was no dynamics prior to the deposition of laser energy. This required, according to the EOS tables used, internal energies in the deposition volume and the water outside it (but within the computational boundaries of our calculation) of IE_I=0.004128 mJ and IE_O=1421.92 mJ, respectively. The large difference in magnitudes of IE_I and IE_O is due to the large difference in these two volumes as represented in the simulation. The energies of importance for understanding the dynamics are the changes in the internal energies, ΔIE_I and ΔIE_O, and the kinetic energies, KE_I and KE_O.

Conservation of energy requires that the sum of IE_I, IE_O, KE_I and KE_O is constant. Table I values satisfy this requirement to a high degree of accuracy.

At 100 ns, approximately 51% of the deposited energy remains in internal energy of the material within the bubble. Approximately 24% resides in the internal energy and 23% in the kinetic energy of the water outside the deposition region. Because of its small mass, well below 1% of the deposition energy resides in kinetic energy of the small mass of water in which the deposition occurred. These simulation results are consistent with the measurements and inferences from the very different analysis procedures of Vogel *et al.*[1] Notice that by 20 ns after the deposition, corresponding to distances less than about 70 μm from the computational axis of symmetry, the internal energy of the water outside the deposition region, ΔIE_O, has reached more than 70% of its value at 100 ns. The temporal behavior of the internal energy deposition is consistent with significant shock dissipation only at very early times in a small region. This too agrees with the analysis of Vogel *et al.*

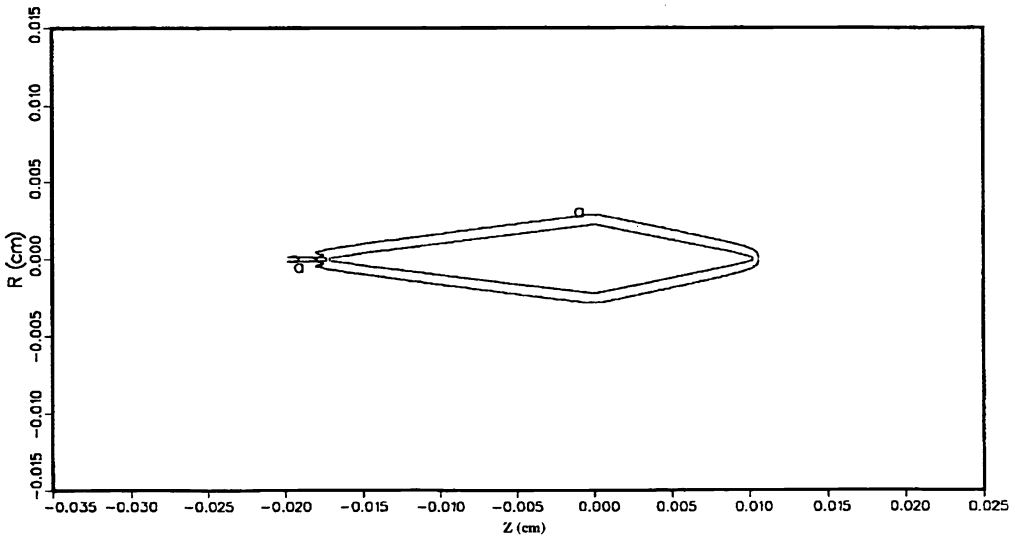

Fig. 4a. The simulated two-dimensional shock wave (represented by the 10 MPa isobar) and bubble wall locations at 2ns for comparison with the MLL photographic record of Fig. 1 and Ref. 1. Figures 4b and 4c are the simulated locations at 20 and 40 ns, respectively.

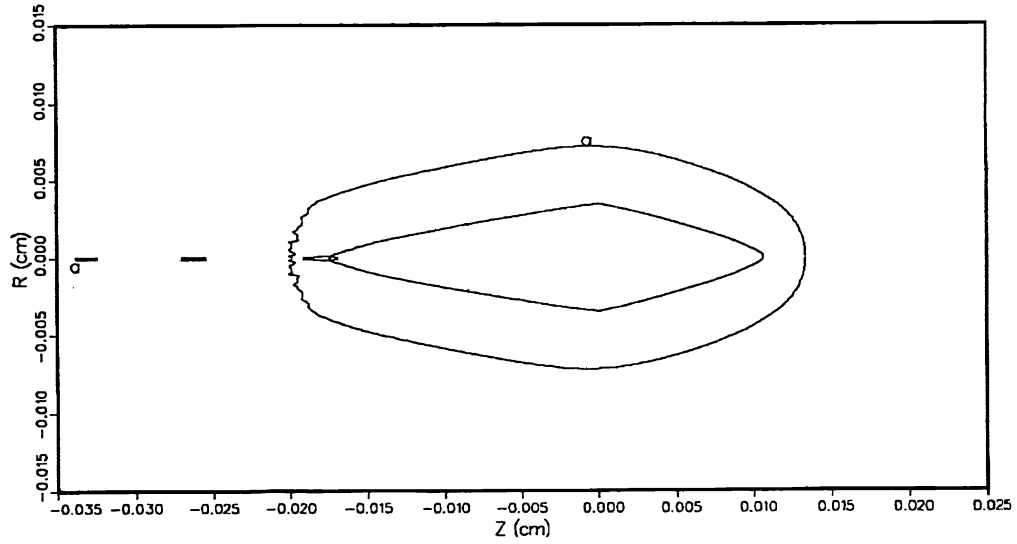

Fig. 4b. Simulation at 20 ns.

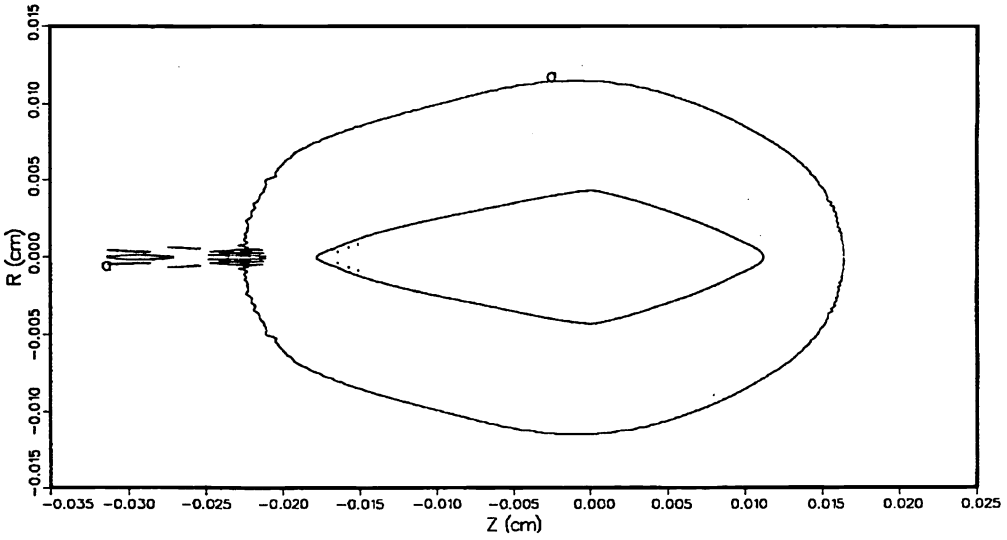

Fig. 4c. Simuation at 40 ns.

4. CONCLUSIONS

We have simulated the dynamics produced by 30-ps 1-mJ laser pulse plasma breakdown in water. The computed shock wave and bubble wall locations as a function of time quantitatively agree with measurements at the MLL. Since the shock wave and bubble wall motion are driven somewhat differently, this excellent agreement validates both the numerical hydrodynamics of the MESA-2D code and the SESAME water equations of state used in the simulations. This agreement also implies that the computed values of the pressure history, the energy residing in various forms, and other important physical quantities are good predictions. Since some of these quantities are difficult to measure directly, especially at early times, our predictions may be useful for those attempting to optimize various protocols for laser medical applications. These results are of immediate value for disciplines, such as ophthalmology, where water is an excellent tissue surrogate. Since many soft tissues have a high water content and a sound speed near that of water, they are also useful guides in estimating the effects of laser deposition in other medical applications.

5. ACKNOWLEDGMENTS

A DOE Cooperative Research and Development Agreement (CRADA) between Los Alamos National Laboratory, Oregon Medical Laser Center, and Palomar Medical Technologies supported both E. J. Chapyak and R. P. Godwin. A. Vogel was supported by the Deutsche Forschungsgemeinschaft. We thank J. D. Johnson of LANL for providing equation-of-state advice.

6. REFERENCES

1. A. Vogel, S. Busch, and U. Parlitz, "Shock wave emission and cavitation bubble generation by picosecond and nanosecond optical breakdown in water," *J. Acoust. Soc. Am.* **100**(1), 148-165, July 1996.

2. U. S. Sathyam, A. Shearin, E. A. Chasteney, and S. A. Prahl, "Threshold and Ablation Efficiency Studies of Microsecond Ablation of Gelatin Under Water," *Lasers in Surgery and Medicine*, **19**, 397-406 (1996).

3. E. J. Chapyak and R. P. Godwin, "Numerical studies of bubble dynamics in laser thrombolysis," in *Lasers in Surgery: Advanced Characterization, Therapeutics, and Systems VI*, R. Rox Anderson, M.D., Editor, Proc. SPIE 2671, 84-87 (1996).

4. L. Likhterov, "High-frequency acoustic noise emission excited by laser-driven cavitation," *J. Fluid Mech.* **318**, 77-84, 1996.

5. R. M. Roberts, J. A. Cook, R. L. Rogers, A. M. Gleeson, and T. A. Griffy, "The energy partition of underwater sparks," *J. Acoust. Soc. Am.* **99**(6), 3465-3475, June 1996.

6. J. G. Kirkwood and H. A. Bethe, "The Pressure Wave Produced by an Underwater Explosion I," OSRD No. 588, May 1942. This classic is difficult to obtain, but has been reproduced unabridged in *John Gamble Kirkwood Collected Works, Shock and Detonation Waves*, ed. W. W. Wood, 1-34, Gordon and Breach, New York, 1967.

7. C. E. Brennen, *Cavitation and Bubble Dynamics*, Chap. 1, Oxford Univ. Press, New York, 1995.

8. K. S. Holian, "T-4 Handbook of Material Properties Data Bases," Los Alamos National Laboratory report LA-10160-MS, 1984.

9. "SESAME: The Los Alamos National Laboratory EOS Data Base," S. P. Lyon and J. D. Johnson, Editors, LA-UR-92-3407, 1992.

10. L. Haar and J. S. Gallagher, "A Thermodynamic Surface for Water: The Formulation and Computer Programs," National Bureau of Standards internal report 81-2253, 1981.

11. K. Nahen and A. Vogel, "Plasma formation in water by picosecond and nanosecond Nd:YAG laser pulses. II. Plasma transmission, scattering and reflection," *IEEE J. Sel. Topics Quantum Electron. Issue on Lasers in Medicine and Biology*, (to be published).